8 Determination of Layer Thicknesses of Single Layers and Multilayers

The measurement of layer thickness is a basic problem, and can be solved both by x-ray reflection and x-ray diffraction (see [121] for a review). In both methods, the thickness of a thin layer can be determined from the angular positions of the subsidiary maxima on the reflection (or diffraction) curves.

In a reflectivity curve, these maxima are caused by the interference of the waves reflected from the upper and lower interfaces of the layers. This phenomenon is equivalent to the interference fringes that can be observed with visible light, known as Pohls interference pattern [128]. The visibility of this interference effect depends substantially on the reflectivities of both boundaries, i.e., on the differences in the x-ray refraction indices above and below the boundaries and on the interface roughnesses. In the x-ray region, the latter factor is especially important since, as we show later, even a very fine roughness on the nanometer scale gives rise to a considerable decrease in interface reflectivity.

The range of the layer thicknesses that can be measured by x-ray reflectometry depends on the intensity and divergence of the primary beam, on the angular resolution, and on the total angular range of the goniometer used, as well as on the wavelength λ (see Chap. 2).

As we show later, in the case of a single layer of the thickness T, the distance between the adjacent interference maxima is given by

$$\delta\eta_i = G\frac{\lambda}{2T}, \tag{8.1}$$

where G is a geometry factor, which is unity for x-ray reflectivity. Therefore, the primary-beam divergence and/or the angular resolution of the diffractometer determines the *upper* limit of the measurable thickness T. If, for instance, the divergence of the primary beam is $0.01°$ and $\lambda = 0.15405$ nm ($\mathrm{CuK}\alpha_1$ line), the maximum measurable layer thickness is smaller than about 0.43 μm. The lower limit for thickness analysis is given by the accessible angular range, i.e., in fact, by the maximum incidence angle α_i that yields a measurable reflectivity. Therefore, the minimum layer thickness which can be determined, depends on how many decades of intensity are accessible by the experiment. For instance, the determination of a layer thickness of 1.5 nm requires measurements up to $\alpha_i = 3°$ at least.

The subsidiary maxima on the diffraction curve of a layered sample can be explained as a result of interference of the beam diffracted by the layer (or layers) with the beam diffracted by the substrate. The distance of the adjacent maxima depends on the layer thickness according to a formula similar to Eq. (8.1), where the value of the geometrical factor G can differ from unity depending on the diffraction asymmetry. The scattering contrast of the interference maxima depends mainly on the difference between the polarizability coefficients χ_h of the layer and the substrate and on the lattice mismatch between layer and substrate. For the latter case the thickness determination is not straightforward and requires computer simulation.

In this chapter we will describe the possibilities for determining the layer thickness in single-layer and multilayer structures by x-ray reflectometry and diffraction measurements. On the basis of the general theory formulated in Sect. 6.5, we will demonstrate the dependence of the positions of the intensity maxima on the reflection (diffraction) curves on the layer thicknesses and we will discuss the influence of the inhomogeneities of the layer thickness on these curves.

8.1 X-Ray Reflection by Single Layers

From general dynamical formulae (6.14), (6.39) we can derive the following expression for the reflectivity of a single layer deposited on a semi-infinite substrate:

$$\mathcal{R} = \left| \frac{r_1 + r_2 \mathrm{e}^{-2\mathrm{i}k_{0z}T}}{1 + r_1 r_2 \mathrm{e}^{-2\mathrm{i}k_{0z}T}} \right|^2 , \tag{8.2}$$

where $r_{1,2}$ are the Fresnel reflectivity coefficients of the free surface and the substrate interface, respectively, k_{0z} is the vertical component of the wave vector of the beam transmitted through the layer, and T is the layer thickness. From this formula it follows that in an angle-dispersive experiment the intensity maxima appear whenever $\exp(-2\mathrm{i}k_{0z}T) = 1$, this means at angle positions α_{im}. This condition can be expressed by

$$2T\sqrt{\sin^2 \alpha_{im} - \sin^2 \alpha_c} = m\lambda, \tag{8.3}$$

where m is an integer, $\sin \alpha_c = \sqrt{2(1-n)}$ and α_c is the critical angle of total external reflection of the layer and n is the layer refractive index. Eq. (8.3) is analogous to the Bragg equation but modified by the influence of refraction. The appearing thickness fringes are called *Kiessig fringes*, in honor of their discoverer [193].

Since, in most cases, the incidence angle α_i is sufficiently small, Eq. (8.3) has the following approximative form:

$$\alpha_{im}^2 - \alpha_c^2 = m^2 \left(\frac{\lambda}{2T} \right)^2 . \tag{8.4}$$

This relation shows a simple method to determine the layer thickness from the measured reflectivity curve. One plots the squares of the angular positions of the intensity maxima versus the squares of the Kiessig fringe order. In the range of validity of Eq. (8.4) it gives a straight line with the layer thickness T as parameter. From the intersection point of this straight line with the ordinate one obtains the critical angle α_c of the layer material, and, consequently its refractive index.

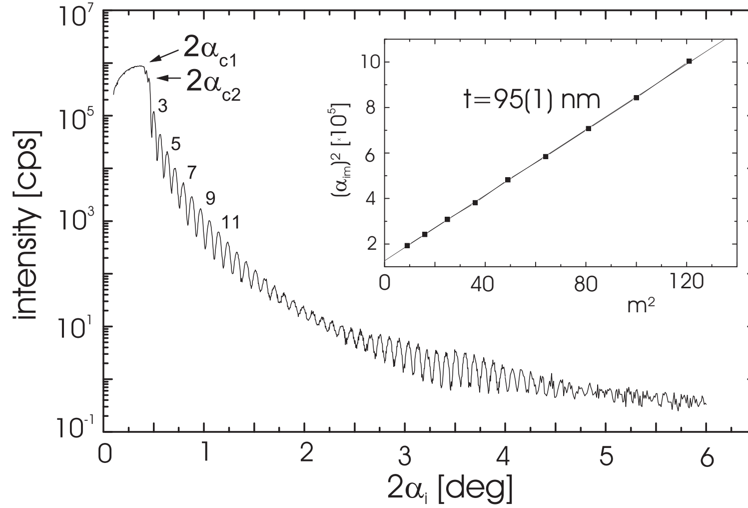

Fig. 8.1. X-ray reflectivity curve of BN coated onto silicon substrate recorded as a function of the detector angle $2\alpha_i$. α_{c_1} is the critical angle of the layer; α_{c_2} that of the substrate. The numbers denote the fringe order m. The inset shows the plot α_i^2 versus m^2, which gives a layer thickness of $T = 95 \pm 1$ nm.

Figure 8.1 shows a reflectivity curve of a BN layer deposited on a silicon substrate. It was measured by means of a powder x-ray diffractometer introduced in Chapter 2.4 using $\lambda = 0.154$ nm. The reflected intensity is recorded over six orders of magnitude. This corresponds to $2\alpha_i \leq 6.0°$.

For intensity reasons and to improve the angular resolution, the low angle region between $0 < 2\alpha_i < 2\alpha_c$ was measured with the highest angular resolution possible, what is determined by a step width of $\delta\alpha_i = 0.001°$ and a width of the incident beam of 0.05 mm. A counting time of 2 seconds per angular step was sufficient for good counting statistics. For larger α_i the slit width and the counting time were increased to 0.5 mm and 30 to 60 seconds, respectively. As is visible in Fig. 8.1 the intensity increases slightly for $\alpha_i < \alpha_c$ and drops very rapidly if α_i exceeds α_c. The first dependence is governed by the *illumination correction* (see later).

Beyond α_c the reflected intensity is proportional to α_i^{-4} as follows from the kinematical formula (5.17). This drop is modulated by the interference of the x-ray beam reflected at the upper and lower boundaries of the layer. Furthermore, there are two different frequencies of oscillations. The high frequency is a measure of the thickness of the sputtered BN layer, and the low frequency is that of the native SiO_2 covering the silicon substrate. The layer thickness T of the BN is obtained from the angular distance between the oscillation maxima according to (8.4). This is demonstrated in the inset of Fig. 8.1 using the third to eleventh Kiessig maximum of the reflection curve. Its graphical evaluation gives $T = 95 \pm 1$ nm. The extrapolation to $m = 0$ gives $\alpha_{c1}^2 \approx 10^{-5}$, which represents a rough estimate of the average electron density of the layer. α_{c2} corresponds to the density of the silicon substrate (see below). Extracted from the long-range beating of the reflectivity curve, the thickness of the SiO_2 layer amounts to 3.4 ± 0.4 nm. Note that this layer becomes visible only if the reflectivity curve has been recorded over more than five orders of magnitude.

Expressed in reciprocal space, Eq. (8.3) looks much simpler:

$$T = \frac{2\pi}{\Delta Q_{zT}}. \tag{8.5}$$

That means T can be measured from a difference of the scattering vectors *inside* the crystal (i.e., corrected for refraction).

The accuracy of the thickness determination depends on the smallest angular step $\delta\alpha_i$ of the goniometer and on the layer thickness T. Neglecting refraction the accuracy can be estimated from

$$\frac{\Delta T}{T} = \frac{\Delta\alpha_i}{\alpha_i} \approx \frac{\alpha_i}{m_{\max}}. \tag{8.6}$$

This accuracy is of the order of 1% if the oscillation maximum measured at $\alpha_i = 1°$ is determined with an accuracy better than $\Delta\alpha_i = 0.01°$. Eq. (8.6) can be expressed also in terms of the largest fringe order $m_{\max}$ that is detected in the reflectivity curve with an accuracy of one-half of a fringe period. In the example shown in Fig. 8.1 one finds $m_{\max} = 45$ at $2\alpha_i \approx 5.0°$. In this case the layer thickness t is determined with a relative error of $\frac{\Delta T}{T} \approx 2\%$.

The accuracy of the layer thickness can be preserved as long as a sufficient number of fringe maxima appear within the detectable angular interval, i.e., if T is sufficient large. Owing to the α_i^{-4} dependence, the reflectivity of the silicon substrate decreases to $\mathcal{R} = 2 \times 10^{-4}$ at $2\alpha_i = 2°$ and to $\mathcal{R} = 5 \times 10^{-5}$ at $2\alpha_i = 3.0°$. Considering the low counting statistics at large angles, the thickness cannot be estimated with an accuracy better than 1% in practical cases. A dynamical range of up to ten orders of magnitude is required in order to detect one single fringe period corresponding to the thickness of a single atomic layer ($T \approx 0.3$ nm). Such dynamical range cannot be realized under common laboratory conditions, it requires synchrotron radiation . Nowadays, a dynamic range of seven to eight orders of magnitude is available using modern home laboratory equipment (see Sect. 2.1).

However, using a low-power x-ray source, a rough estimate of the layer thickness of a very thin layer can be determined exploiting the small-angle part of the reflectivity curve, in particular the angular position of the first oscillation minimum [382].

The electron density of the material can be determined by measuring the critical angle of total external reflection α_c. From theory (see Chap. 6) one would expect the reflecting intensity to remain constant between $0 < \alpha_i < \alpha_c$. That is not the case in experiments: as seen in Fig. 8.1, the intensity increases within this angular range. For a given beam width, b_{beam}, and a very small α_i, the projection of the incoming beam onto the sample surface, A_{beam}, can exceed the sample size, A_{sample} (see Fig. 8.2) . Under this condition the recorded intensity depends on the ratio $b_{\text{sample}}/b_{\text{beam}}$ and has to be corrected by

$$\begin{aligned} I &= I_{\text{meas}} \cdot \sin(\alpha_i) \quad \text{for } \frac{A_{\text{sample}}}{A_{\text{beam}}} < 1 \\ &\text{and} \\ I &= I_{\text{meas}} \quad\quad\quad\quad \text{for } \frac{A_{\text{sample}}}{A_{\text{beam}}} \geq 1 \,. \end{aligned} \tag{8.7}$$

The particular angle α_i, where $A_{sample}/A_{beam} = 1$, depends on the sample size and the slit width b_{beam} defining the beam in front of the sample. Both parameters have to be defined for each sample under investigation. A correct

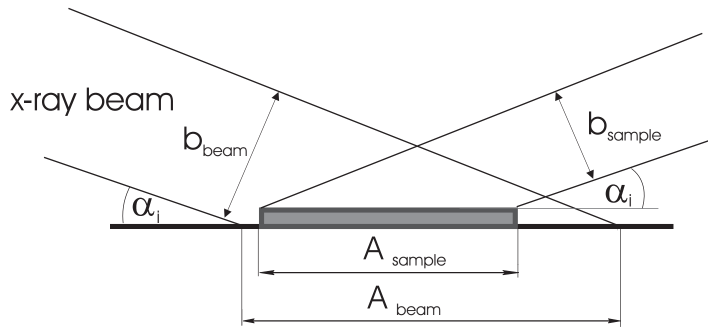

Fig. 8.2. Illumination of a terminated sample area while scanning the reflectivity at very small α_i.

determination of α_c is not straightforward. As long as absorption is negligible and the sample is infinitely large, α_c is that value of α_i where the reflecting intensity I_c is decreased to 50% compared of the maximum intensity $I_{\max} = 1$. In this case $I_{\max}$ corresponds to the incident beam intensity I_0 measured at $\alpha_i = 0$. For finite-sized samples and highly absorbing materials I_{max} is always smaller than unity and α_c appears at an intensity smaller than 50% (see Eq.

(8.7)). This problem becomes significant if the electron density of the layer is lower than that of the substrate and if the layer is thin. Then two critical angles may appear: one belongs to the layer and a second one, at slightly larger α_i, corresponds to the substrate. This has already been illustrated in Fig. 8.1.

Generally the average electron density ϱ_{el} can be determined using the relation

$$\alpha_c = \sqrt{-\chi_0}, \tag{8.8}$$

which results in

$$\varrho_{\mathrm{el}} = \frac{\pi \alpha_c^2}{\lambda^2 r_{\mathrm{el}}}. \tag{8.9}$$

Instead of ϱ_{el} the mass density ϱ_{m} is often of interest. These two densities are connected by

$$\varrho_{\mathrm{m}} = \frac{\varrho_{\mathrm{el}} A}{N_A Z}, \tag{8.10}$$

where r_{el} is the electron radius defined in Sect. 5.1, Z is the atomic number, A is the mass number and N_A is the Avogadro constant. Figure 8.3 shows three

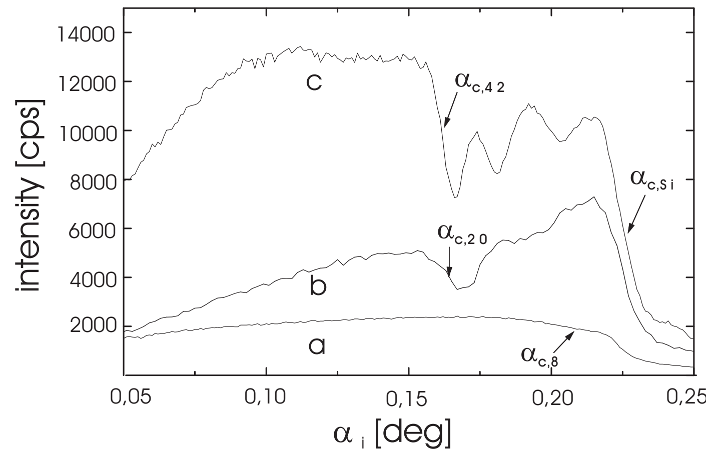

Fig. 8.3. The angular range of total external reflection, recorded for three different organic films made of from fatty acid salt molecules coated onto a silicon support by means of the Langmuir-Blodgett technique. As can be seen here, the critical angle of film decreases as the number of layers increases due to the increased number of structural defects within the film.

reflectivity curves of organic films made of different numbers of monolayers coated onto a crystalline silicon support. Besides the critical angle of silicon

at 0.22°, there is a second α_c which belongs to the organic film. This smaller critical angle decreases with an increase in the number of monolayers, due to the increasing number of defects within the layer. For the 20–monolayer sample, for example, $\alpha_c = 0.18°$ corresponds to an electron density of $\varrho_{\rm el} = 4.6 \times 10^{23}$ cm^{-3}, i.e., a mass density of $\varrho_{\rm m} = 1.54$ gcm^{-3}. The density values of the silicon substrate are 6.99×10^{23} cm^{-3} and 2.32 gcm^{-3}, respectively. A density determination by eye is not possible if the layer density is close to that of the substrate or if the layer is very thin. The latter reason is evident in the bottom curve of Fig. 8.3. Here, the layer density can only be extracted using computer simulation. In that particular example, the decreasing density of the layer is caused by the incomplete layer coverage on the substrate which decreases with the number of transferred layers [353].

For an approximate determination of $\varrho_{\rm el}$, we recommend measuring the reflectivity curve in the angle range $0 \leq \alpha_i \leq 1.5 \times \alpha_c$ using the smallest possible step width of the goniometer $\delta\alpha_i$ and find α_c at the angle position where $I(\alpha_i) = I_{\rm max}/2$. Using $\delta\alpha_i \sim 0.001°$, the accuracy of the density determination may be estimated as

$$\Delta\varrho/\varrho = 2\frac{\delta\alpha_i}{\alpha_c} \sim 0.01 \ , \tag{8.11}$$

which is sufficiently precise for many technological applications. This procedure works well if the rotational axis of the sample circle is aligned exactly at the sample surface (see Sect. 2.1).

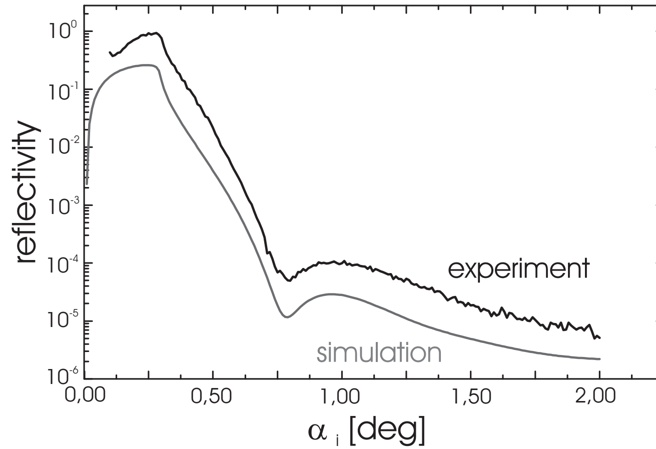

Fig. 8.4. Experimental and fitted x-ray reflectivity curves of a thin antimony layer on GaAs (110) substrate. The experiment cannot be explained assuming a single-layer model.

The following examples will illustrate some problems one may encounter while studying extremely thin layers. Figure 8.4 shows the reflectivity curve of a thin antimony layer grown epitaxially on GaAs (110) . This curve was recorded using a reflectometer with low angular resolution. It demonstrates the limit of layer thickness estimation made by eye. The electron density of antimony is about 15% larger than that of GaAs. Therefore the critical angle of the layer is larger than that of the substrate and it is not visible. At larger angles a single fringe minimum and maximum are visible above the background, the shape of the oscillation is asymmetric. A complete fit of the reflectivity curve which considers the experimental resolution function gives $T_{Sb} = (4.0 \pm 0.5)$ nm, an interface roughness of $\sigma = 0.5$ nm and a refraction index $n \approx 1 - \delta$ with $\delta_{Sb} = 1.65\ 10^{-5}$. The interface roughness was treated according to Sect. 11.3. Additionally one has to consider a second layer with slightly reduced density ($\delta = 1.05\ 10^{-5}$) on the top of the antimony. Its thickness is about $T = (2.8 \pm 0.5)$ nm, and it corresponds to microcrystalline aggregates caused by the transition of the two-dimensional into the three-dimensional growing mode during preparation.

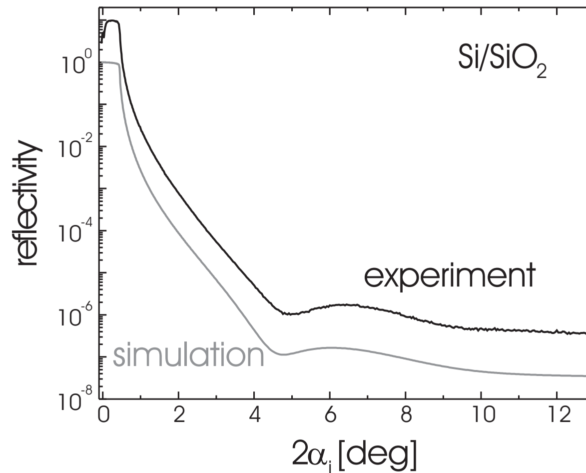

Fig. 8.5. Experimental simulated reflectivity curves of a silicon surface measured with the use of a home reflectometer similar to that shown in Fig. 2.1. The enhanced dynamical range of the experiment enables us to determine a thin top layer of native oxide. The thickness of the native oxide is 1 nm with a surface roughness of about 0.35 nm. The fit is possible only considering a gradual increase of the electron density from oxide to the pure silicon.

This exact data evaluation is in contrast to a rough estimate by eye. Here one can suppose a single-layer model. Using the fringe minimum at $\alpha_i = 0.76°$, one get a thickness of $T = (9 \pm 1)$ nm, which is larger than the sum of both layers determined above. Naturally this model does not reproduce the observed fringe asymmetry [144].

The lower limit for the determination of a thin surface layer can be estimated measuring the native oxide of a silicon wafer. Figure 8.5 shows the reflectivity curve of a *clean* silicon surface measured with a home reflectometer similar to Fig. 2.1 using $\lambda = 0.154$ nm. The experimental curve is quite similar to that one which can be measured with synchrotron radiation [167, 356]. Only the large dynamical range of about eight orders of magnitude makes it possible to identify the native oxide. The measured angular position of α_c corresponds to the silicon mass density of $\varrho_{\rm m} = 2.32$ g/cm^3. At higher α_i the intensity decrease is modulated due to the existence of a very thin surface layer. At the angular position of the destructive interference the reflecting intensity is about 10^{-7}. Under circumstances of a limited dynamical range the reflection curve would probably have been misinterpreted by a clean surface only. Here one clearly can identify the existence of the native oxide. The minimum at $2\alpha_i \approx 4.8°$ corresponds to a thickness of $T_{\rm top} = 1.0$ nm. The full fit of the reflectivity curve supplies additional parameters, i.e., the mass density of the top layer($\varrho_{\rm m} = 1.7$ g/cm^3) and the interface roughnesses of the SiO_2 surface and the SiO_2-Si interface, which are $\sigma_{\rm Si} = 0.15$ nm and $\sigma_{\rm SiO_2} = 0.35$ nm, respectively. Furthermore the fit requires consideration of a gradual change of the density from the top layer down to the pure silicon. This reflects the property of SiO_2 to protect the silicon against further oxidation.

After the substrate has been characterized, the layers on top of it can be investigated. This can be a thin organic film, as shown in Fig. 8.6. The layer consists of lipids(l-1,2-dipalmitoylphosphatidic acid – DPPA) attached to polyelectrolyte molecules (poly-diallyldimethylammonium chloride – PDADMAC). Both have been transferred onto a silicon substrate by means of the Langmuir-Blodgett technique. The main problem here is the low density difference between the molecular sub-units. Both lipids and polyelectrolytes consist of carbon and hydrogen atoms. The only difference is the molecular arrangement which is laterally ordered in the case of the lipids but rather random for the polyelectrolyte molecules. The reflectivity curve has to be recorded over eight orders of magnitude to yield sufficient structure information (Fig. 8.6). As shown in the inset, the data evaluation does not result in a unique electron density distribution. Assuming either a two-layer or a four-layer model, one cannot decide whether the polyelectrolytes built the sub-layer with larger or smaller thickness compared to the lipid layers [271]. This ambiguity is a consequence of the *phase problem* of crystallography.

Similar information can be obtained using the energy-dispersive set-up (see Sect. 2.1). Instead of the angular coordinate the intensity varies as a

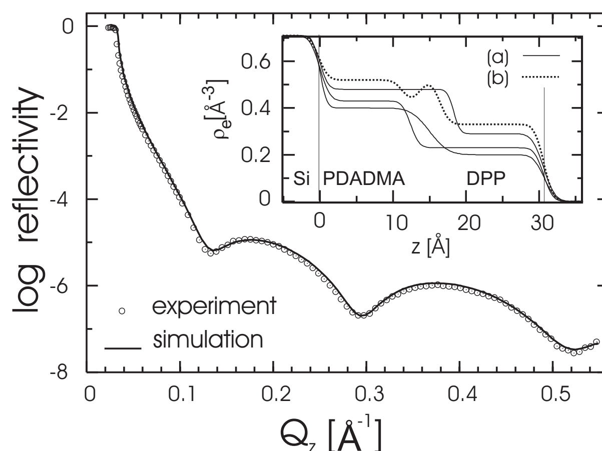

Fig. 8.6. X-ray reflectivity curve of a lipid monolayer attached to a polyelectrolyte molecule. Both are covered onto silicon support. Although the fit to the experimental curve is perfect there is an ambiguity with respect to the correct electron density distribution. This problem cannot be solved without additional structural information. The inset displays the fitted vertical density profile, (a) two box model, (b) four box model.

function of energy at fixed α_i. Figure 8.7 shows reflectivity spectra taken from a lipid monolayer of DPPA spread onto a water surface. The experiment has been performed onto a Langmuir through installed at the sample position shown in Fig. 2.3 at an energy-dispersive beamline. The incoming beam is reflected first at two super-mirrors (see Fig. 1.12) using an incident angle of $\alpha_i = 0.25°$ in each case. This provides an incidence angle of 2° with respect to the water surface. The reflectivity spectra mainly reflect the reflectivity of the super-mirror, which gives an almost uniform intensity up to about 16 keV, multiplied with the incident spectrum of the storage ring. There is a distinct difference in reflectivity between the spectra taken from the pure water surface and from the film on water. After division of the film spectrum by the water spectrum one can clearly identify one maximum and one minimum between $4 \leq E \leq 13$ keV. Both change as a function of the applied lateral surface pressure π. The thickness of $T = 3.2$ nm at $\pi = 40$ and 29 mN/m corresponds to a phase where the molecules stand upright with respect to the water surface. At $\pi = 11$ mN/m, the minimum and maximum shift toward higher energies. The respective thickness of $T = 2.9$ nm corresponds to a phase of tilted molecules. Each spectrum was recorded for 300 seconds. This time is sufficient to observe in-situ phase transitions of various amphiphilic molecules on the water surface as a function the applied pressure.

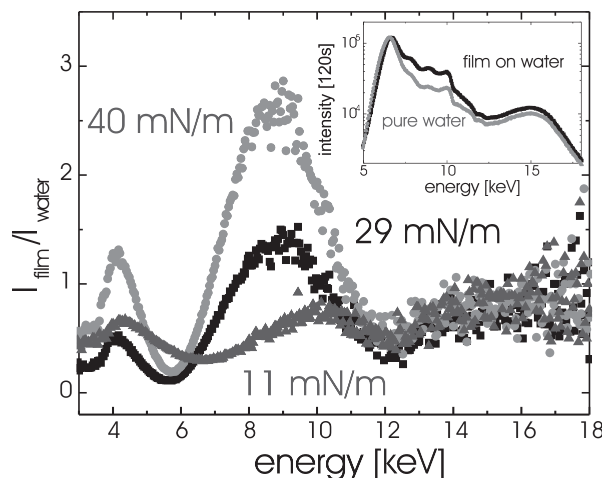

Fig. 8.7. Energy-dispersive reflectivity spectra taken from a lipid monolayer onto the water surface. The experiment is performed on a Langmuir trough when a lateral pressure π can be applied to the molecules spread onto the water surface. The reflectivity spectrum (see inset) mainly corresponds to that of the super-mirror shown in Fig. 1.12. The main figure displays the normalized spectra taken at three different values of lateral pressure. The first minimum and second maximum of the monolayer reflectivity is visible. Their positions at $\pi = 40$ and 29 mN/m correspond to a phase where the molecules stand upright with respect to the surface; $\pi = 11$ mN/m reflects a phase of tilted molecules.

8.2 X-Ray Reflection by Periodical Multilayers

Up to now, we have dealt with systems containing one or two layers. We have demonstrated that the parameters of the system consisting of a single layer on a substrate can be estimated from the measured reflectivity curve by eye. A simple analysis of the experimental reflectivity curve is possible if the sample consists of a periodical stack of layers (a periodical multilayer).

The x-ray reflectivity of a periodical multilayer can be calculated using the kinematical theory, or, more exactly, using Eq. 6.37 in the dynamical theory presented in Chap. 6. In many cases, the single-reflection approach (SRA) is quite sufficient. In this approach we neglect multiple reflections from different interfaces within the multilayer, and for the reflectivities of the interfaces we use the exact dynamical expressions (Fresnel coefficients – see Eq. (6.14)). In the following, we analyze the SRA formula in order to discuss some characteristic features of the reflectivity curve of a periodical multilayer.

Let us assume a multilayer being created by N periods, each consisting of a layer A with a thickness T_A and the refraction index $n_A = 1 - \delta_A$ and the layer B ($T_B,\ n_B = 1 - \delta_B$); the multilayer period is $D = T_A + T_B$. We denote the appropriate phase factors of layers A and B by

$$\Phi_S = \mathrm{e}^{-\mathrm{i}k_z^S T_S},\ S = A, B,$$

where k_z^S is the z-component of the wave vector of the transmitted wave in the layer of type S. For the Fresnel reflection coefficients of the A–B and B–A interfaces, the relation

$$r_{BA} = -r_{AB}$$

holds, i.e., the amplitude of the reflection originating from the interface A–B is opposite that of the interface B–A. Using the matrix expression (6.37) and neglecting all the terms containing the second and higher powers of the Fresnel reflectivities, the reflectivity of the periodical multilayer is

$$\begin{aligned} \mathcal{R} = \Big| r_{0A} + r_{AB} \big[\Phi_A^2 - \Phi_A^2 \Phi_B^2 + \Phi_A^2 \Phi_B^2 \Phi_A^2 - \cdots \\ \cdots + (\Phi_A^2 \Phi_B^2)^{N-1} \Phi_A^2 \big] + r_{BS} (\Phi_A^2 \Phi_B^2)^N \Big|^2 , \end{aligned} \tag{8.12}$$

where r_{0A} and r_{BS} are the Fresnel reflection coefficients of the free sample surface (interface between the vacuum and layer A) and the substrate surface (interface between layer B and the substrate). The sum (in the square brackets) can be evaluated, and we obtain

$$\begin{aligned} \mathcal{R} = \Big| r_{0A} + \tfrac{r_{AB} \Phi_A^2 \Phi_B^2 (\Phi_A^2 - 1)(\Phi_A^2 \Phi_B^2)^{N-1} + \Phi_B^2 - 1}{(\Phi_A \Phi_B)^2 - 1} + \\ + \mathrm{r}_{BS} (\Phi_A^2 \Phi_B^2)^N \Big|^2 . \end{aligned} \tag{8.13}$$

Using the SRA it is straightforward to derive parameters which characterize the multilayer structure. Several of these parameters can simply be extracted from the experimental reflection curves and can be used as an input for the fitting of the experimental reflection curves by means of full dynamical theory according to Eq. (6.37).

First, let us consider the second term on the right-hand side of formula (8.13). A maximum of this term occurs if

$$(\Phi_A \Phi_B)^2 = 1,$$

i.e., for

$$k_z^A T_A + k_z^B T_B = \pi m,$$

where m is an arbitrary integer. Now we introduce the averaged z-component of the wave vector:

$$\langle k_z \rangle = \frac{k_z^A T_A + k_z^B T_B}{D},$$

making an angle $\langle\alpha_t\rangle$ with the internal surface normal. The condition for a reflectivity maximum is

$$2D\langle n\rangle\sin\langle\alpha_t\rangle = m\lambda, \tag{8.14}$$

where $\langle n\rangle$ is the average refractive index of the multilayer or, using the angle of incidence,

$$2D\sqrt{\sin^2\alpha_i - \sin^2\langle\alpha_c\rangle} = m\lambda. \tag{8.15}$$

This formula is equivalent to Eq. (8.3) for a single layer; but in (8.15) the critical angle of total external reflection $\langle\alpha_c\rangle$ depends on the refraction index averaged over the multilayer period.

As in the case of a single layer, the modified Bragg law can be simplified if the angles are sufficiently small:

$$\alpha_{im}^2 - \langle\alpha_c\rangle^2 = m^2\left(\frac{\lambda}{2D}\right)^2. \tag{8.16}$$

Formulas (8.14) and (8.15) represent the modified Bragg law; and, consequently, optical reflection from a periodical multilayer can be interpreted as a *diffraction* from a one-dimensional crystal. The Bragg equation (8.15) is corrected by the refraction of x-rays in an averaged medium that replaces the actual multilayer structure. The reflectivity maxima can be considered as satellite maxima close to the reciprocal lattice point 000.

If one neglects the refraction, the distance of the satellite maxima can be approximated to

$$\Delta\alpha \approx \frac{\lambda}{2D},$$

which similar to (8.1).

The intensity of the satellite maxima are influenced by the thicknesses T_A and T_B of the layers in the period. The envelope curve of these maxima is described by the structure factor of the one-dimensional crystal, i.e., the multilayer period that, in the case of reflection, has the form

$$F_{\text{period}}(G) = \int_{-D}^{0} \mathrm{d}z\chi_0(z)\mathrm{e}^{-\mathrm{i}Gz} = \frac{\mathrm{i}}{G}(\chi_{0B} - \chi_{0A})\left(\mathrm{e}^{-\mathrm{i}GT_A} - 1\right), \tag{8.17}$$

where $G = \frac{2\pi m}{D}$ is the value of Q_z in the m-th satellite. Like the diffraction case already explained in Chapter 5, the m-th satellite peak vanishes, if the layer thicknesses $T_{A,B}$ obey the following relation:

$$m = p\left(\frac{T_A}{T_B} + 1\right), \tag{8.18}$$

where p is an integer. For instance, every fourth satellite maximum vanishes if $T_A/T_B = 3$.

Now, let us investigate the first and the third terms in Eq. (8.13). These terms provide a maximum of the reflectivity if $(\Phi_A \Phi_B)^2 = 1$; i.e., a maximum occurs for the angles $\langle \alpha_t \rangle$ given by the relation

$$2ND\langle n \rangle \sin\langle \alpha_t \rangle = p\lambda, \tag{8.19}$$

where p is an integer. Neglecting refraction, the angular spacing between these maxima,

$$\Delta\alpha \approx \frac{\lambda}{2ND},$$

is inversely proportional to the *total thickness* $T = ND$ of the multilayer stack. The nature of these maxima (Kiessig fringes) is obvious. They are caused by the interference of the waves reflected at the free surface and at the substrate interface. Simple consideration shows that $N-2$ Kiessig fringes occur between two neighboring satellite maxima. Often the Kiessig fringes are not visible due to lateral sample inhomogeneities.

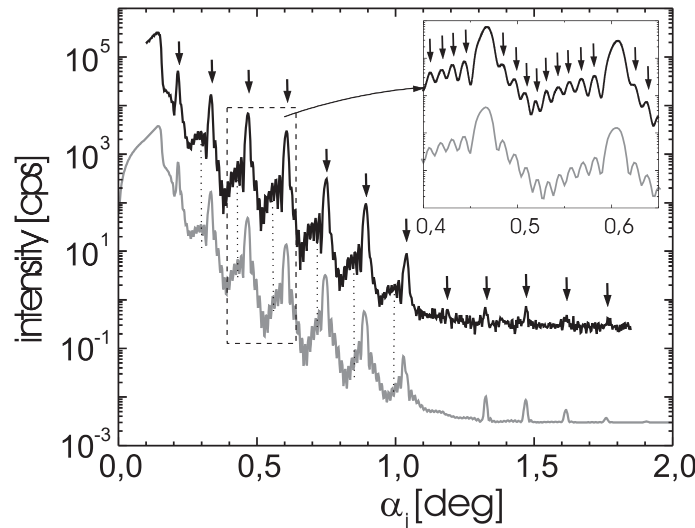

Fig. 8.8. Reflection curve of a SiGe/Si multilayer covered by 210-Å-thick cap layer, CuKα radiation. The satellite maxima are denoted by *vertical arrows*, the maxima stemming form the capping layer are denoted by *vertical dotted lines*. In the inset, the Kiessig fringes corresponding to the total thickness of the multilayer are denoted by *arrows*.

As an example, we show the measured reflection curve of a SiGe/Si multilayer (Fig. 8.8) covered by a Si capping layer with thickness T_C. On the experimental curve, three types of maxima can be resolved:

1. Satellite maxima (indicated by vertical arrows in the main part of Fig. 8.8, whose angular spacing depends on the multilayer thickness D according to (8.15).
2. Kiessig fringes (indicated by the vertical arrows in the inset). Their period depends on the total multilayer thickness $T = ND + T_C$ according to (8.19).
3. Maxima indicated by vertically dotted lines correspond to the thickness T_C of the capping layer.

Knowing the positions of the maxima of these types, we can estimate the corresponding thicknesses using the modified Bragg law in Eqs. (8.15) and (8.19).

Similar to the treatment shown in Fig. 8.1, we have plotted the square of the angular positions of the respective maxima versus the m^2 and obtained the thicknesses $D = (20.5 \pm 0.3)$ nm, $T = ND + T_C = (232 \pm 5)$ nm, and $T_C = (21 \pm 2)$ nm.

These values can serve as starting estimates for the numerical fitting of the whole measured curve using the dynamical theory presented in Sect. 6.4. The result of the fit procedure also is shown in Fig. 8.8. In order to obtain a good correspondence between the measured and calculated curves, we had to assume an oxide layer on top of the multilayer stack (having the thickness T_{ox}). From the fit we obtained the thicknesses of the individual layers as well as the average root mean square roughness σ of their interfaces. The fitting procedure was almost insensitive to the Ge concentration x in the SiGe layers. The fit yielded the following values: $T_{ox} = (3 \pm 1)$ nm, $T_C = (21 \pm 0.5)$ nm, $D = (20.6 \pm 0.2)$ nm, $T_A/T_B = 7.0 \pm 0.2$, $x = 0.35 \pm 0.15$, and $\sigma = (0.7 \pm 0.1)$ nm. The interface roughnesses were considered using the formalism presented in Sect. 11.2.

We can see that the estimates of the layer thicknesses from the positions of the reflectivity maxima nearly coincide with the more reliable values obtained by the numerical fit to the whole curve. The thickness of the additional oxide layer, however, could be estimated with an relative error of only about 30%, because no respective intensity maxima could be identified within the angular range of the measurement.

Figure 8.9 displays the reflectivity curve of a vanadium/mica multilayer sputtered onto a sapphire substrate measured at a wavelength of $\lambda = 0.139$ nm. Due to the huge difference of the electron densities between both constituents the reflectivity at the first-order Bragg peak is close to unity. Thus the multilayer can be used as broad band monochromator for synchrotron radiation use. The accepted band pass depends on the peak width, i.e., the number of coated double layers. In the present case there are 40 periods, which can be verified by the 38 Kiessig oscillations measured between two neighboring Bragg peaks (see inset of Fig. 8.9). The multilayer period amounts to 3.5 nm. The reflectivity curve could be recorded over nine orders of magnitude. The 7th-order Bragg peak appears at $\alpha_i \approx 9°$. Using

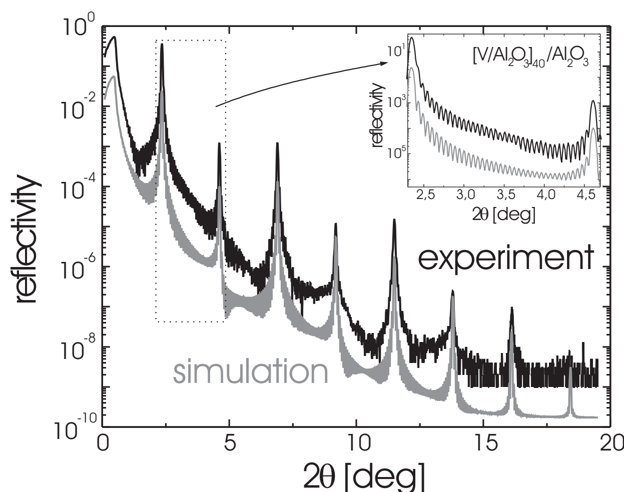

Fig. 8.9. Reflectivity curve of a V/Al_2O_3 multilayer film coated on mica. The experiment has been performed at $\lambda = 0.139$ nm using synchrotron radiation. The reflectivity could be recorded over nine orders of magnitude. The inset shows the angular range between the 1st- and 2nd-order Bragg peak [247].

Eq. (8.6) this corresponds to a relative error of about 2%. The thicknesses of the vanadium and mica layers have been determined by curve simulation and amount to 1.61 nm and 1.87 nm, respectively. The interface roughnesses were determined to be 0.24 nm and 0.18 nm. The substrate roughness amounts to 0.17 nm.

The following example shows a typical reflectivity curve of an organic film. It consists of 28 cadmium–behenate monolayers transferred onto silicon support by means of the Langmuir–Blodgett technique. The behenic acid molecules are amphiphilic in nature. They consist of a hydrophilic COO^- head and a $(CH_2)_nCH_3$ tail. One Cd^{2+} ion is attached to two molecular head groups. This is the reason that a single period of the multilayer always consists of two monolayers of upright standing molecules where the head groups are coupled via the Cd^{2+} ion. Figure 8.10 shows the respective reflectivity curve measured by a powder diffractometer and Cu$K\alpha$ radiation. There are two types of periodic maxima: the main satellites measure the period thickness. Due to the large resonant diffuse scattering (see Chap. 11) which appears in addition to the coherent scattering, these small-angle Bragg peaks are visible over a large angular range. In the present case they appear up to the 14th-order. The multilayer period could be determined as $D = 6.020 \pm 0.006$ nm. The inset of the figure shows the evaluated electron density profile. The pecularity of the multilayer consists in the large density difference between the

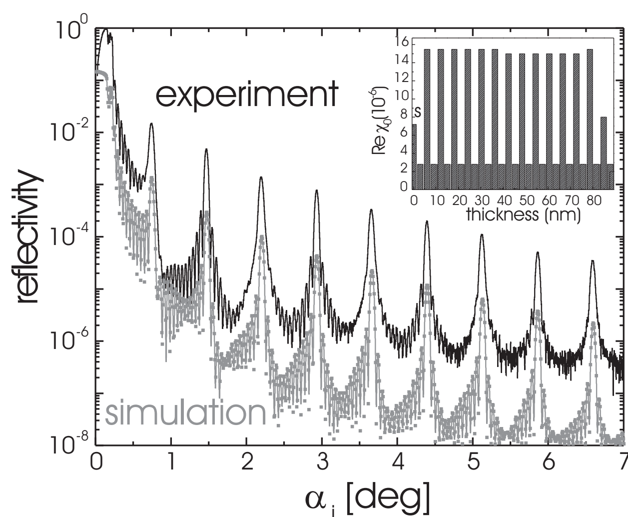

Fig. 8.10. Reflection curve of a 29-monolayer Cd-behenate film deposited on silicon support, measured with CuKα radiation. There are two distinguished series of satellite maxima: the main satellite maxima, measuring the multilayer spacing which consists of two monolayers with opposite molecular orientation, and the Kiessig fringes, measuring the total thickness of the film. Note the large difference in intensity of Kiessig peak maxima left and right with respect to the first satellite maximum which is created by the odd number of monolayers within the film. Curve simulation reveals that there is a fluctuation in the density of the individual sublayers.

chains and the head groups. The head groups are about 0.2 nm thick, but they have a density which is twice as large as that of the silicon substrate. On the other hand, the hydrocarbonic chains have a density of less than one-half of that of the silicon.

Kiessig maxima are clearly visible between the main satellites. Their number is $N = 12$; i.e., the total thickness should correspond to 14 double layers. The evaluation of the angular spacing between the Kiessig maxima results in a thickness of $T = 90.15 \pm 0.35$ nm which corresponds to 15 double layers. This discrepancy has two causes. Due to the hydrophilic nature of the silicon surface the molecules of the first monolayer are deposited with the head straight down to the substrate. Therefore, this layer is not a part of a double layer and the film consists of 29 monolayers. This non-centrosymmetry becomes visible as the strong asymmetry in the Kiessig intensities on left and right with respect to the first main satellite [283]. A second reason for the larger total thickness is the molecular pile-up effect; a few molecules leave the molecular layers and jump on top of the film, creating islands. Because this process is already associated with a very small activation energy at room

temperature, a sufficient number of molecules alter their vertical positions within the multilayer film, increasing the total film thickness as a function of time [108].

Finally one can determine the average density of the organic film. As in Fig. 8.3, the critical angle of the films is smaller than that of the silicon substrate. From $\langle \alpha_{c,\mathrm{film}} \rangle = 0.175°$, one obtains an average density of $\varrho_\mathrm{m} = 1.5\ \mathrm{gcm}^{-3}$. Note there are Kiessig maxima in the angular range between the critical angles of film and substrate. This effect is similar to that already shown in Fig. 8.3. Figure 8.11 shows a similar organic multilayer, a cadmium

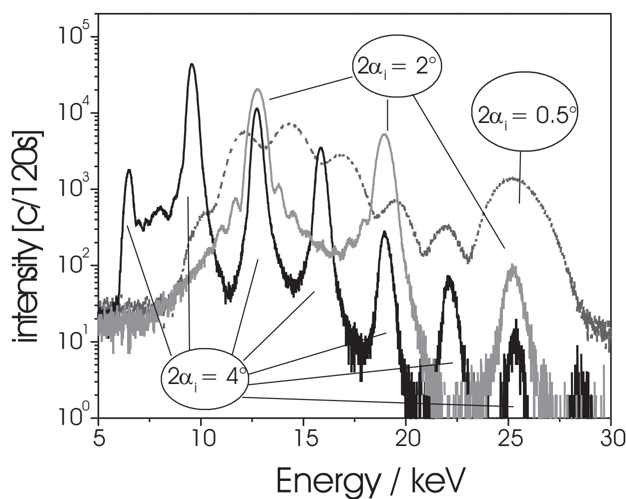

Fig. 8.11. Energy-dispersive reflection curves of a cadmium-behenate multilayer film measured at different incidence angles. The counting time per spectrum was 120 seconds each. The number of Bragg peaks increases with increasing α_i. Due to the limited detector resolution the Kiessig fringes disappear at large α_i.

behenate multilayer film covering a silicon substrate. Here, the experiment has been performed at the energy-dispersive beamline at BESSY II. As introduced in Sec. 3.2, the accessible range of the reflectivity curve depends on the incidence angle. For $\alpha_i = 0.5°$, the range between the first and second-order Bragg peak is probed. Several Kiessig fringes and the second-order Bragg peak are visible. The first-order Bragg peak is attenuated due to the large absorber thickness used to protect the detector. More Bragg peaks become visible, increasing the incidence angle. Eight Bragg peaks appear for $\alpha_i = 4°$, but no Kiessig fringes. This is due to the fact that the peak width now is determined by the limited detector resolution. Due to the different absorber

thicknesses used, the onset of the reflectivity differs between the spectra measured at different α_i.

The layer thickness and total thickness can be determined from the peak distance at the energy scale. In energy-dispersive reflectometry the Kiessig peak maxima and Bragg peaks appear at different energies, changing α_i due to the relation $q_z E$. Rewriting Eq. (8.3) in terms of energy, the energy spacing ΔE between two neighboring intensity maxima decreases for increasing α_i. The layer thickness T follows from

$$\delta E = \frac{hc}{2T \sin \alpha_i} \approx \frac{6.2}{T\alpha_i}, \tag{8.20}$$

where h and c are the Planck constant and the velocity of light, respectively. Refraction is neglected in Eq. (8.20) and $\sin \alpha \approx \alpha$. The accuracy of the thickness determination depends on the energy resolution of the detector ΔE:

$$\frac{\Delta T}{T} = \frac{\Delta E}{E}. \tag{8.21}$$

For a germanium or Si:Li detector ΔE is about 180 eV. This results in a relative accuracy of $\frac{\Delta T}{T} \sim 1\%$ for peaks measured at $E = 10$ keV. The upper limit for evaluating a layer thickness depends on the minimum separation which can be resolved between two peaks. Assuming $\Delta E = 0.5$ keV and $\alpha_i = 0.25°$, the limit amounts to about 300 nm. The limited energy band pass of the experiment determines the lower limit of the thickness determination. Using $\alpha_{i,\max} = 4°$ and a band pass of about 15 keV, the lower limit is on the order of 1 nm. This limit has been determined by measuring the thermal expansion coefficient of polymer films with thicknesses of about 100 nm [48].

The evaluation of spectra shown in Fig. 8.11 gives a multilayer period of $D_{LB} = 5.65 \pm 0.05$ nm and a total thickness of $T_{\text{tot}} = 56$ nm, which verifies preparation conditions. The comparison of the various spectra manifests the validity of Eq. (8.20). As seen, the number of the Bragg peaks is doubled, increasing α_i by a factor of two.

In comparison with the angle-dispersive set-up, the accuracy of the absolute thickness determination is lower. Nevertheless each spectrum shown in Fig. 8.11 was collected in 120 seconds which is a small fraction of the time necessary for recording the analogous angle-dispersive curves.

8.3 Coplanar X-Ray Diffraction by Single Layers

X-ray reflection is sensitive to the gradient of the electron density normal to the air-sample interface; that means the layer thickness can be determined independent of crystal perfection. In contrast to this, coplanar x-ray diffraction measures the lattice spacing of the layer as well, presuming crystalline perfection. Therefore, it is advantageous to combine reflection and diffraction measurements in order to obtain complete information on the investigated